


## Research Article

# Genetic Mechanism of Lower-Order Faults in Shale Formations in Rift Basins

Haimeng Yang,<sup>1,2</sup> Xuepeng Wu,<sup>3</sup> Jingshou Liu ,<sup>4</sup> and Caifu Hu<sup>5</sup>

<sup>1</sup>State Key Laboratory of Shale Oil and Gas Enrichment Mechanisms and Effective Development, SINOPEC, Beijing 100083, China

<sup>2</sup>College of Earth Sciences and Engineering, Shandong University of Science and Technology, Qingdao 266590, China

<sup>3</sup>SINOPEC Research Institute of Petroleum Engineering Co., Ltd., Beijing 102206, China

<sup>4</sup>School of Earth Resources, China University of Geosciences, Wuhan 430074, China

<sup>5</sup>Tongren Zhongneng Natural Gas Co., Ltd., Tongren 554300, China

Correspondence should be addressed to Jingshou Liu; [liujingshou@126.com](mailto:liujingshou@126.com)

Received 26 October 2022; Revised 21 November 2022; Accepted 18 March 2023; Published 19 April 2023

Academic Editor: Peng Tan

Copyright © 2023 Haimeng Yang et al. This is an open access article distributed under the Creative Commons Attribution License, which permits unrestricted use, distribution, and reproduction in any medium, provided the original work is properly cited.

The distribution of lower-order faults affects the development of oil and gas and the distribution of remaining oil, which is also the key to the development of fault block reservoirs in eastern China. The lower-order faults are characterized by short extension, small fault displacement, and difficult identification by traditional seismic interpretation methods. Therefore, it is necessary to predict the development law of faults in combination with the paleostress field during the fault formation period to improve the accuracy of fault seismic interpretation. In this paper, on the basis of reservoir structural analysis and rock mechanics experiments, the geological and mechanical model of the Sanduo period is established to predict the simulation of the paleostress field during the development of lower-order faults. The development of lower-order faults in rift basins is mainly controlled by the minimum principal stress and stress difference, and the shear stress in the profile controls the tendency of faults. Controlled by the paleostress field, the occurrence of lower-order faults in the Weizhuang area, Gaoyou Sag, and Subei Basin is very complex, and the strike of the fault is distributed as a tension shear broom on the plane. The prediction results can provide a reference for the excavation of remaining oil and the development of oil and gas.

## 1. Introduction

Complex fault block oilfields are widely distributed in China, with complex internal fault systems. Faults of different orders control the formation and distribution of oil and gas in fault block oilfields [1–3]. Higher-order faults control the structural trend and occurrence of the fault block, thus controlling the formation and accumulation of oil and gas. The existence of lower-order faults further complicates the fault block oilfield and is an important controlling factor for remaining oil enrichment [4–7]. With the exploration and development of oil fields, the excavation of remaining oil has become the primary content of increasing production and tapping potential of oil fields. Therefore, it is of great theoretical and practical significance to study the development law of lower-order faults. Any fault relative to the fault

with a higher order can be called a lower-order fault, which specifically refers to the fourth- and fifth-order faults in oil-field development [1, 4, 7, 8]. The lower-order faults are characterized by short extension and small fault displacement, basically not controlling the accumulation of oil and gas, and it is difficult to identify accurately in seismic data, thus becoming a key point in the fine description of high water cut reservoirs. Because its formation is mainly controlled by the local tectonic stress field, analyzing the local regional stress field becomes an important method to predict lower-order faults [1, 8–10].

At present, some new seismic technologies, such as 3D seismic fine interpretation, fine coherence analysis, and seismic attribute technology, are mainly used to realize the identification and description of lower-order faults [3, 4, 7]. On the basis of identification and description, methods such as

the structural background method, fault combination analysis method, structural stress field analysis method, structural physical simulation method, and rock stratum curvature method are mainly used to predict the development law of lower-order faults, thus guiding the implementation of local structures [1, 8]. Shale deformation can be determined through physical simulation and numerical simulation in combination with synchronous CT and thin section observations [11–13]. Geomechanical modeling is an effective method for predicting the large-scale deformation of shale [13–18]. According to 3D structural maps and rock mechanics experiments, a geomechanical model can be established to simulate the paleostress field in different periods [1, 2, 19]. In this paper, on the basis of 3D seismic interpretation, the authors apply the numerical simulation method of the tectonic stress field to simulate the distribution of paleotectonic stress and then predict the plane and profile development laws of lower-order faults from the perspective of stress. Finally, the latest structural map is used to reveal the genetic mechanism of lower-order faults.

## 2. Geological Setting and Stratigraphy

**2.1. Geological Setting.** The Weizhuang area is located west of the Hanliu fault zone in the Gaoyou Sag, Subei Basin (Figure 1), which is the stress release area of the Hanliu fault zone. The distribution of faults in this area is extremely complex, and it is a narrow fault nose structure group that is uplifted from south to north. The main oil-bearing series are the 2nd member ( $E_1f^2$ ) and the 1st member of the Funing Formation ( $E_1f^1$ ). It has been nearly 30 years since the region was put into development in 1996. At present, all of them have entered the stage of a medium-high water cut, and development is becoming increasingly difficult. The two challenges faced by oilfield development are as follows: the degree of oil recovery is increasing, the reserves are insufficient, and stable production requires the replacement of new fault blocks. However, due to the poor seismic data, it is difficult to implement the structure. Second, after multiple rounds of adjustment and densification, the well pattern in the main part is relatively complete, with little room for further improvement [8, 20, 21].

The region was developed in 1996 and has been developed for nearly 30 years. At present, all of them have entered the stage of high water content, and the difficulty of development has become increasingly difficult. The two challenges facing oilfield development are as follows: first, the degree of oil recovery is increasing, reserves are insufficient, and stable production requires new fault blocks to replace, but due to poor seismic data, it is difficult to implement the structure. Second, after multiple rounds of adjustment and densification, the well pattern in the main part is relatively complete, with little room for further improvement [8, 20, 21].

**2.2. Stratigraphy.** Gaoyou Sag has nearly 7000 m thick strata from the Upper Cretaceous to the Quaternary, which is the sag with the largest sedimentary thickness and the most fully developed strata in the Subei Basin. The Paleogene strata are the main oil generation strata and are mainly composed of

continental clastic deposits (Figure 2) [8, 20, 21]. The Hanliu fault zone is developed in the sedimentary cover of the Gaoyou Sag. The Mesozoic Cenozoic strata cut through from bottom to top are the Paleogene Funing Formation, Dainan Formation, Sanduo Formation, Neogene Yancheng Formation, and Quaternary Dongtai Formation. The target horizon studied in this paper is the second member of the Funing Formation ( $E_1f_2$ ). The lithology is mainly gray black and dark gray mudstone mixed with marlstone, thin limestone, dolomite, and a small amount of shale in the upper part, and light gray siltstone and gray black mudstone are interbedded in varying thickness in the lower part, with an apparent thickness of 33~300 m.

**2.3. Tectonic Evolution.** From the first to fourth members of the Funing Formation, the fault activity gradually increased during the sedimentary period, and the number of active faults reached a maximum in the Dainan period; during the sedimentation period of the Sanduo Formation, the fault activity peaked, and the number of active faults in the deep depression zone decreased. Based on comprehensive analysis of stratum thickness, structural evolution profile, fault activity law, etc., the structural evolution of the Hanliu fault zone can be divided into four stages [8]: the sedimentary period of the first and third members of the Funing Formation is the stage controlled solely by the Zhen-1 fault (Figure 1); the sedimentary period from the fourth member of the Funing Formation to the second member of the Dainan Formation is the formation and development stage of the Hanliu fault; during the sedimentation period of the Sanduo Formation, the Hanliu fault zone was complicated and controlled by two faults (Neogene-Quaternary depression development period). During the sedimentation of the Funing Formation, the fault strike is generally close to the E-W direction, indicating that the direction of the minimum principal stress in the Funing Formation is close to the N-S direction. The stress direction of the sedimentary period of the Sanduo Formation is basically consistent with the orientation and stress direction of active faults during the sedimentary period of the Funing Formation.

Influenced by the interaction between the paleostress field and the faults in the surrounding areas, according to the observation and statistical results of core fractures, the fractures in the study area are mainly near east-west and northeast fractures. High-angle fractures and vertical fractures account for more than 80% of the total fractures. The true opening of macro fractures is mainly distributed between 0.3 mm and 0.6 mm, the linear fracture density is small, and the development degree of fractures between wells varies greatly. Most structural fractures are filled with calcite, and some oil shows and a small amount of argillaceous filling. Tensile, shear, and tensile-shear joints are developed (Figure 3).

## 3. Data and Methods

**3.1. Numerical Simulation of the Stress Field.** Numerical simulation is an effective method for analyzing tectonic stress fields, and finite element simulation is a more commonly

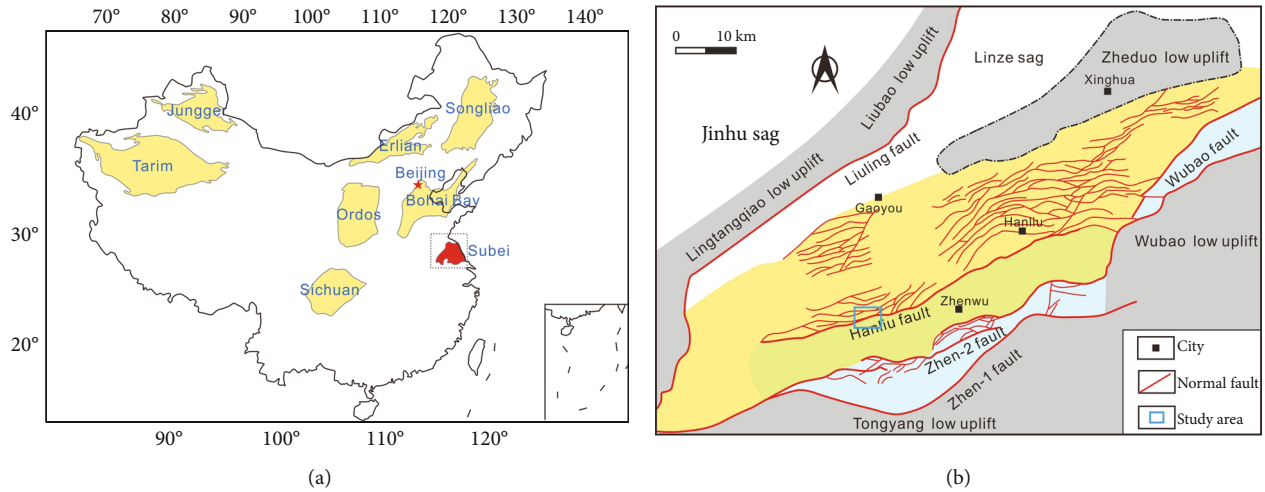


FIGURE 1: (a) Tectonic location of the Subei Basin. (b) Tectonic location of the Weizhuang area and fault system of the Gaoyou sag. The red line represents normal faults (modified according to [1]). Different colors represent different tectonic units.

Erathem	System	Formation	Member	Formation code	Thickness (m)	Age (Ma)	Tectonic movement
Cenozoic	Quaternary	Dongtai formation		$Qd$	0-300	2.0	Sanduo movement
	Neogene	Yancheng formation	Member 2	$Ny^2$	100-900		
			Member 1	$Ny^1$	100-700		
	Paleogene	Sanduo formation	Member 2	$E_2s^2$	50-800	24.6	
			Member 1	$E_2s^1$	100-800	45.0	
		Dainan formation	Member 2	$E_2d^2$	100-900	50.5	
			Member 1	$E_2d^1$	0-750	53.0	
		Funing formation	Member 4	$E_1f^4$	0-500	54.9	
			Member 3	$E_1f^3$	150-300	56.0	
			Member 2	$E_1f^2$	150-350	58.0	
			Member 1	$E_1f^1$	350-1000	60.2	
	Mesozoic	Cretaceous	Taizhou formation	Member 2	$K_2f^2$	150-250	
Member 1				$K_2f^1$	150-300	75.0	
						83.0	Yizheng movement

FIGURE 2: Stratigraphy and tectonic movement in the Gaoyou Sag (modified according to [1]).

used method [19, 22, 23]. The finite element method is a numerical solution method to approximate the general continuum problem. Its basic idea is to simplify the studied continuum into a discrete model composed of finite elements and then apply the computer to solve the numerical solution. A geological body is discretized into finite continuous elements, which are connected by nodes, and each element is given with its actual rock mechanical parameters. We convert the solution of the continuous field function in the study

area to the solution of field function values at a finite number of discrete points (nodes), and the basic variables are displacement, strain, and stress [19, 23–26]. According to the boundary stress conditions and node equilibrium conditions, establish and solve the equations with node displacement as the unknown quantity and the overall stiffness matrix as the coefficient. The interpolation function is used to obtain the displacement on each node, and then, the stress and strain values in each element are calculated [27–32].



FIGURE 3: Fracture development characteristics of the Subei Basin. (a) Shear fractures developed in mudstone of Well S10, filled with mud, 2300.61 m. (b) Shear fracture developed in mudstone of Well J2, filled with calcite, 2231.52 m. (c) Shear fracture developed in mudstone of Well S10, unfilled, 2288.01 m. (d) Tensile fracture developed in mudstone of Well S10, 2308.21 m. Due to the requirement of confidentiality of oilfield data, we did not display the actual well name.

These elements are combined to calculate the tectonic stress field of the whole geological body. With the increase in the number of elements, the model is closer to the actual geological body, and the results of numerical simulation need to be measured and evaluated by certain inspection standards to judge the effectiveness and accuracy of simulation. However, the paleostress field is a stress field in a certain historical period. At present, there is no effective way to evaluate them, and there is no mature and reliable test standard for its results. In general, successful paleostress field simulation should at least reach the following two points: the simulated stress field should correspond well with the tectonic intensity of the simulated area, and the simulation results can be used to explain the nature and intensity of tectonic activity [8, 33]; the simulated stress value should conform to the objective geological laws, and the relationship between the stress value and the rock strength, burial depth, structural characteristics, and other factors should be fully considered to

ensure the validity and accuracy of the simulation results of the stress field [34–36].

**3.2. Calculation Method of Rock Strain Energy.** According to the theory of elasticity, strain energy accumulates in the solid during deformation, and the strain energy in the solid can be measured by the strain energy density [37, 38]:

$$\omega = \frac{1}{2}(\sigma_1 \varepsilon_1 + \sigma_2 \varepsilon_2 + \sigma_3 \varepsilon_3). \quad (1)$$

In equation (1),  $\sigma_1$ ,  $\sigma_2$ , and  $\sigma_3$  are the principal stresses corresponding to the element and  $\varepsilon_1$ ,  $\varepsilon_2$ , and  $\varepsilon_3$  are the corresponding stress directions. Both theory and experiments have proven that sandstone, siltstone, and shale show strong brittleness. The maximum strain energy criterion for brittle rock fracture considers that when the release rate of elastic strain energy accumulated inside is equal to the energy



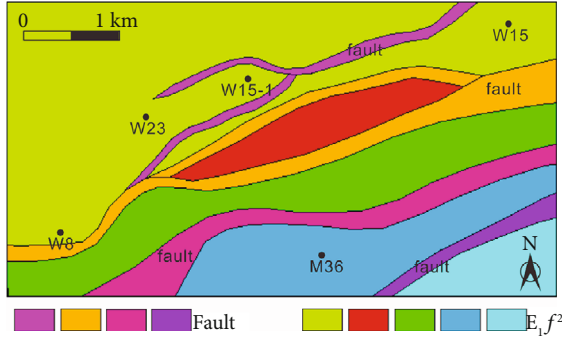


FIGURE 4: Geological model of the Weizhuang area.

required to produce the surface of the fracture body per unit area, the brittle material will fracture [39, 40].

### 4. Results

**4.1. Geologic Model.** Through seismic interpretation, the fracture map and structural relief of shale tops in the study area are obtained. According to the bottom structure map of the second member of the Funing Formation, the model is simplified, and the preexisting high-order faults are selected to establish the geological model of the Weizhuang area (Figure 4). The main strike of the fault in the study area is NEE, and the dip angle of the fault is 45°. Thickness is a key factor affecting rock fracture [41] and is closely related to the activity and distribution of high-order faults [42]. According to the logging data, the model is determined as the sand mud interbed model, which is divided into five layers, and the thickness of the model is 150 m. The top and bottom sandstone layers are 40 m, the middle sandstone layer is 30 m, and the thickness of the two sets of mudstone layers is 20 m.

**4.2. Geomechanical Model.** The mechanical properties of different tectonic units are different. The strength of the general fault zone is weaker than that of the normal sedimentary strata [25, 28, 30]. The strength of the new strata in the sag area is greater than that of the old strata in the bulge area. According to the actual situation of the fault zone, the fault is assigned a mechanical parameter, and the rest of the sedimentary stratum is assigned a unified value of the mechanical parameter of the stratum. The size of the rock mechanical parameter is referred to in some experimental tests (Table 1). On the basis of loading mechanical parameters, the Solid45 element in ANSYS [23] is used for grid division, and 25986 elements are divided, with 16299 nodes participating in the operation (Figure 5). The Solid45 element is 8 nodes, each element is a cube, and nodes are 8 vertices on the cube. The external force acting on the cube element shall be loaded through the node. The external force does not act on the element directly but deforms the cube element through the node. The element is applicable to the numerical simulation of the stress field of a layered structure.

According to the analysis of paleostress and strain, the model loading is constantly changed. Finally, it is deter-

TABLE 1: Mechanical parameters of the structural stress field simulation in the Weizhuang area.

	Poisson's ratio	Young's modulus (GPa)	Rock density (kg·m <sup>-3</sup> )
Shale	0.15	28.5	2210
Sandstone	0.18	24.3	2270
Fault	0.20	22.0	2200

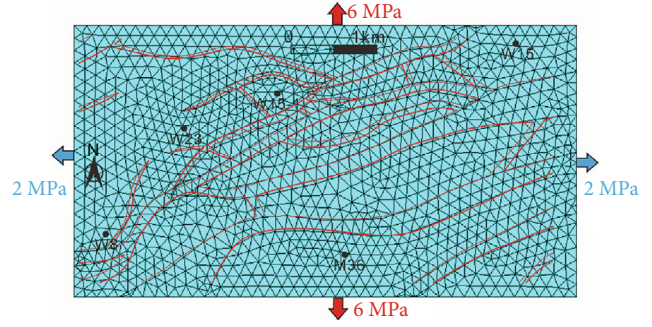


FIGURE 5: Geomechanical model and stress boundary conditions of the Sanduo period in the Weizhuang area.

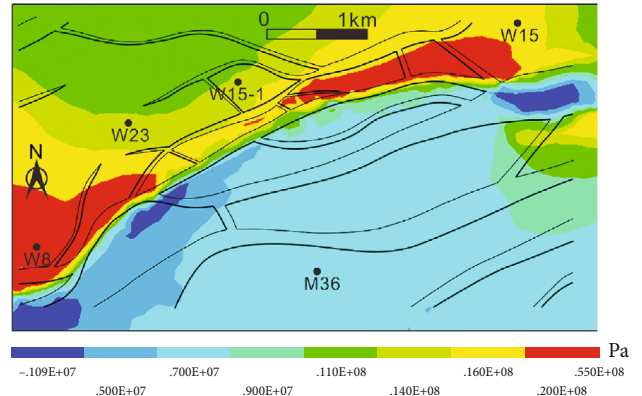


FIGURE 6: Distribution diagram of the minimum principal stress in the Weizhuang area (negative values represent compressive stress).

mined to apply 9.8 m/s<sup>2</sup> gravity acceleration to the model during the Sanduo Period. Taking the rotation direction of the plane of the preexisting high-order fault in this period as the macroconstraint condition and meeting the requirements of finite element analysis and calculation, a tensile stress of 6 MPa is applied to the north-south boundary, a tensile stress of 2 MPa is applied to the east-west boundary, and a shear stress of 2 MPa is applied to the east boundary of the model to ensure the convergence of the calculation results and apply east-west linear constraints to the model frame (Figure 5). In addition, the Z direction displacement constraint of the bottom of the model is set to zero.

**4.3. Numerical Simulation Results of the Stress Field.** Using ANSYS software, the maximum principal stress distribution diagram and the minimum principal stress distribution diagram of the study area are obtained after solving. As shown

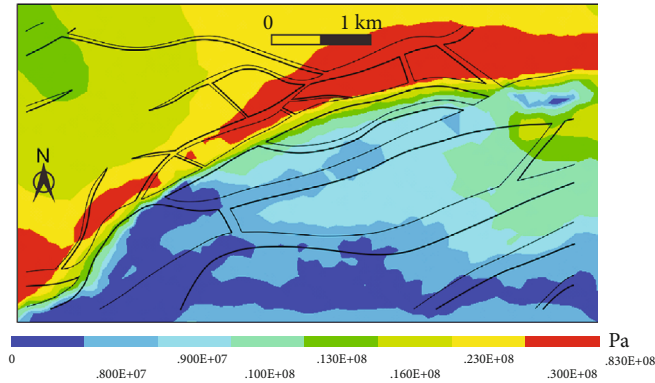


FIGURE 7: Relationship between stress difference and fault development.

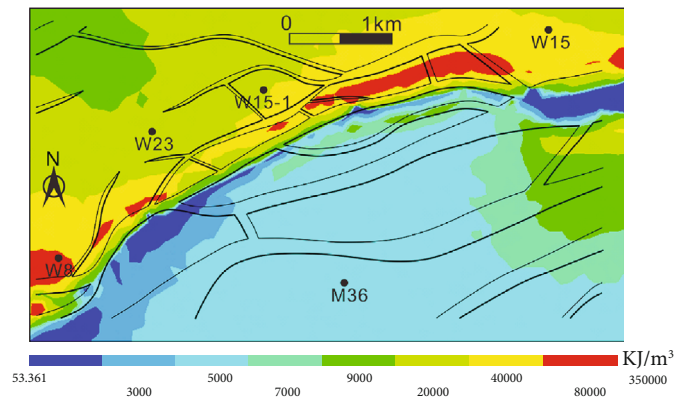


FIGURE 8: Relationship between strain energy and fracture development.

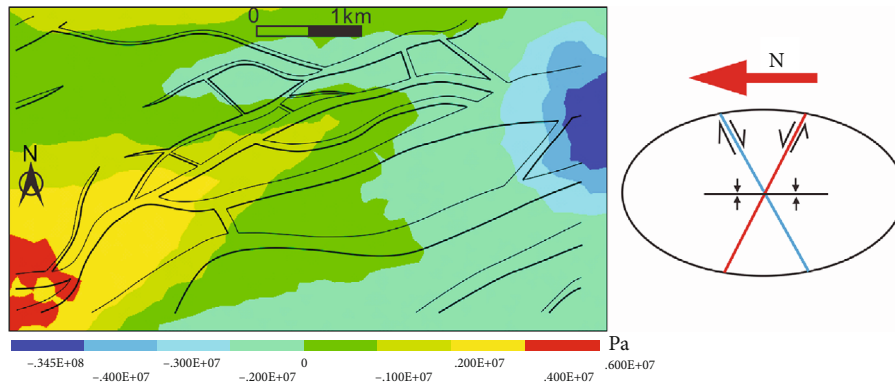


FIGURE 9: Correspondence between the lower-order fault tendency and profile shear stress in the Weizhuang area (negative values represent dextrorsal shear stress).

in Figure 6, due to the strike-slip effect of the fault, the minimum principal stress is high in the hanging wall of the fault and low in the southeastern and southern parts of the study area. The intermediate principal stress is the nearly east-west principal stress. Due to the strike-slip action of the fault, the minimum principal stress is high in the hanging wall near the fault and low in the southwestern and southern parts of the study area.

## 5. Discussion

**5.1. Development Degree of Lower-Order Faults.** As shown in Figure 7, the difference between the maximum principal stress and minimum principal stress is high in the footwall of the fault, and the stress is 3-8 MPa; at the hanging wall of the fault, i.e., the southwest and south of the study area, the stress is low, and the stress is 0-1 MPa.

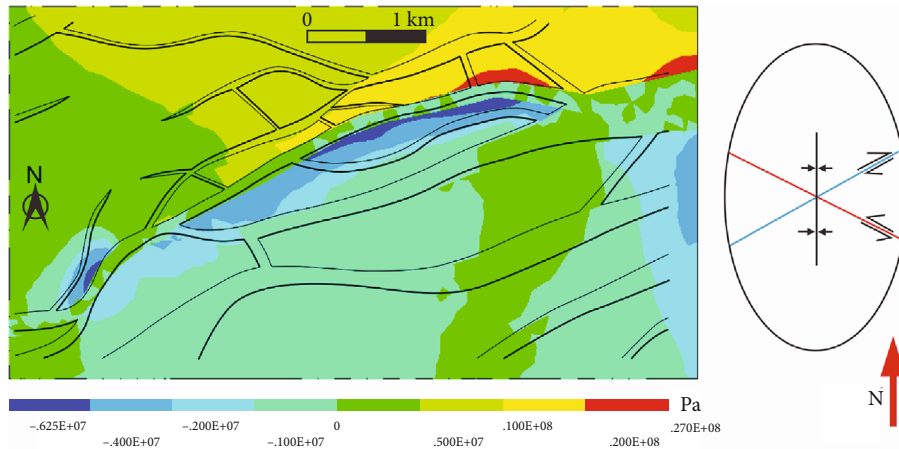


FIGURE 10: Correspondence between the strike of lower-order faults and plane shear stress in the Weizhuang area (negative value represents right rotation).

As shown in Figure 8, the distribution of strain energy is similar to the distribution of stress difference, showing high values in the footwall and low values in the hanging wall of the fault. In the area of high strain energy, the probability of rock fracture is higher; in contrast, the probability of rock fracture is small.

5.2. Development Law of the Lower-Order Fault Tendency.

Figure 9 shows the distribution relationship between the lower-order fault tendency and the profile shear stress in the Weizhuang area, where negative values represent dextral shear stress and south-dipping fault development areas; a positive value represents a sinistral direction and a north-dipping fault development area. The middle and eastern parts of the study area are generally inclined to the south, while the southwestern part is generally inclined to the north. The simulation results are basically consistent with the trend of lower-order faults, indicating that the shear stress of the profile controls the lower-order fault tendency.

5.3. Strike Development Law of Lower-Order Faults.

As shown in Figure 10, the footwall of the Hanliu fault is of sinistral shear stress, with NNE-NE trending faults developed. The strike of low-order faults is nearly perpendicular to the minimum principal stress. The hanging wall of the fault is dextral shear stress, developing NE-trending faults. In the southwestern part of the study area, the footwall of the fault is dextral shear stress, developing NNE-trending faults.

As shown in Figure 11, the minimum horizontal principal stress in the Weizhuang area is near the north-south tensile stress. Because the rotation direction of plane shear stress near the fault changes, the stress near the fault deflects in different directions. At the footwall of the fault, the stress direction is NNE and nearly north-south at the footwall of the fault. Near the fault, the horizontal minimum principal stress direction rotates to a certain extent, and the stress direction turns parallel to the fault strike.

The method proposed by [1] is used to quantitatively predict the strike of small faults in this area. The intermedi-

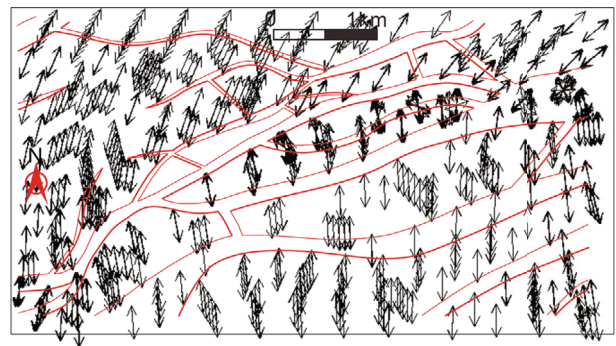


FIGURE 11: Direction of the horizontal minimum principal stress in the Weizhuang area.

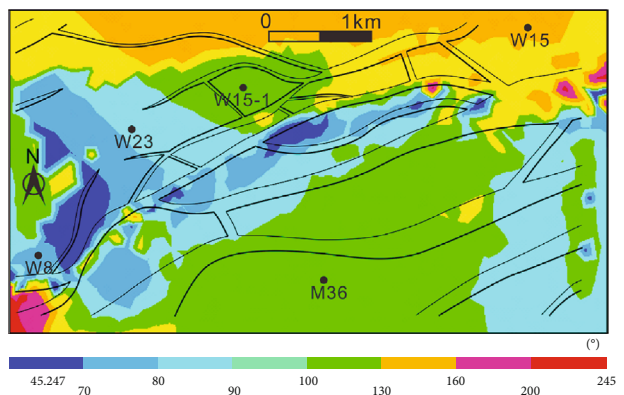


FIGURE 12: Prediction results of the strike of lower-order faults in the Weizhuang area.

ate principal stress is mainly used to control the strike of faults. In combination with the direction of paleostress, the strike of lower-order faults in the Weizhuang area is quantitatively predicted through the transformation of the stress coordinate system and geodetic coordinate system (Figure 12). Affected by the Hanliu fault, the Weizhuang area is located in the stress release area of the Hanliu fault.



The strike of the lower-order fault is very complex, and it is distributed in a tension shear broom shape on the plane. The direction gradually changes from NNW to EW and NE. In the southwestern part of the study area, the strike of the lower-order fault changes to nearly NS.

## 6. Conclusions

Geomechanical modeling is an effective means for numerical simulation of paleostress fields and quantitative prediction of lower-order faults. According to the strike of active faults in different periods, the direction of paleostress and fault system can be determined, and the geomechanical model in different periods can be established to effectively predict the paleostress field in different periods.

The development degree of lower-order faults is mainly controlled by the minimum principal stress, strain energy and stress difference. The occurrence of faults is closely related to the stress type and planar and section shear stresses. The shear stress of the profile controls the tendency of the fault.

In the stress release zone near the fracture, the main stress direction is easy to deflect. Influenced by the Hanliu fault, the study area is located in the stress release area of the Hanliu fault, and the strike of lower-order faults is distributed in a tension shear broom shape on the plane. The direction of stress near the fault turns parallel to the fault strike.

## Data Availability

The data that support the findings of this study are available from the corresponding author, Jingshou Liu.

## Conflicts of Interest

The authors declare that they have no conflicts of interest.

## Acknowledgments

This research was supported by the project ZR2020QD035 of the Shandong Provincial Natural Science Foundation, the "CUG Scholar" Scientific Research Funds at China University of Geosciences (Wuhan) (project no. 2022046), and the Open Research Fund of State Key Laboratory of Geomechanics and Geotechnical Engineering, Institute of Rock and Soil Mechanics, Chinese Academy of Sciences, Grant No. SKLGME021023.

## References

- [1] J. Liu, W. Ding, J. Dai, Z. Wu, and H. Yang, "Quantitative prediction of lower order faults based on the finite element method: a case study of the M35 fault block in the western Hanliu fault zone in the Gaoyou Sag, East China," *Tectonics*, vol. 37, no. 10, pp. 3479–3499, 2018.
- [2] J. Liu, H. Yang, K. Xu et al., "Genetic mechanism of transfer zones in rift basins: insights from geomechanical models," *GSA Bulletin*, vol. 134, no. 9-10, pp. 2436–2452, 2022.
- [3] S. Zhang, Y. Wang, D. Shi, H. Xu, X. Pang, and M. Li, "Fault-fracture mesh petroleum plays in the Jiyang Superdepression of the Bohai Bay basin, eastern China," *Marine and Petroleum Geology*, vol. 21, no. 6, pp. 651–668, 2004.
- [4] X. L. Fu and H. G. Zhang, "Numerical simulation of structural stress field in Funing sedimentary period and prediction of the development law of lower-order faults in Chajian slope zone," *Journal of Geomechanics*, vol. 19, no. 2, pp. 125–132, 2013.
- [5] W. He, E. Barzgar, W. Feng, and L. Huang, "Reservoirs patterns and key controlling factors of the Lenghu Oil & Gas Field in the Qaidam Basin, Northwestern China," *Journal of Earth Science*, vol. 32, no. 4, pp. 1011–1021, 2021.
- [6] T. Hu, X. Q. Pang, F. J. Jiang et al., "Key factors controlling shale oil enrichment in saline lacustrine rift basin: implications from two shale oil wells in Dongpu Depression, Bohai Bay Basin," *Petroleum Science*, vol. 18, pp. 687–711, 2021.
- [7] J. B. Zhang, J. W. Feng, T. F. Tian, and C. D. Mao, "Development law and prediction of the lower-order faults in the west of Zhenwu fault zone in Gaoyou sag," *Journal of Geomechanics*, vol. 18, no. 1, pp. 11–21, 2012.
- [8] J. S. Liu, W. L. Ding, J. S. Dai, Y. Gu, H. M. Yang, and B. Sun, "Quantitative multiparameter prediction of fault-related fractures: a case study of the second member of the Funing Formation in the Jinhu Sag, Subei Basin," *Petroleum Science*, vol. 15, no. 3, pp. 468–483, 2018.
- [9] G. B. Chen, T. Li, L. Yang, G. H. Zhang, J. W. Li, and H. J. Dong, "Mechanical properties and failure mechanism of combined bodies with different coal-rock ratios and combinations," *Journal of Mining and Strata Control Engineering*, vol. 3, no. 2, article 023522, 2021.
- [10] W. Li, M. Meng, X. Chen et al., "Quantitative characterization of extension and compression derived from bending strike-slip faults and their petroleum geological significance of the eastern Bohai Sea," *Journal of China University of Petroleum (Edition of Natural Science)*, vol. 45, no. 5, pp. 23–32, 2021.
- [11] Y. G. Ma, C. G. Su, and Y. X. Yue, "Quantitative study of seismic forward modeling affecting the accuracy of low-order fault identification," *Progress in Geophysics*, vol. 35, no. 2, pp. 616–622, 2020.
- [12] H. Zhu, Y. Ju, C. Huang, F. Chen, B. Chen, and K. Yu, "Microcosmic gas adsorption mechanism on clay-organic nanocomposites in a marine shale," *Energy*, vol. 197, article 117256, 2020.
- [13] H. Zhu, Y. Ju, Y. Qi, C. Huang, and L. Zhang, "Impact of tectonism on pore type and pore structure evolution in organic-rich shale: implications for gas storage and migration pathways in naturally deformed rocks," *Fuel*, vol. 228, pp. 272–289, 2018.
- [14] W. Ju and W. Sun, "Tectonic fractures in the Lower Cretaceous Xiagou Formation of Qingxi Oilfield, Jiuxi Basin, NW China. Part two: numerical simulation of tectonic stress field and prediction of tectonic fractures," *Journal of Petroleum Science and Engineering*, vol. 146, pp. 626–636, 2016.
- [15] X. Liu, C. Xiao, S. Zhang, and B. Chen, "Numerical modeling of deformation at the Baiyun gold deposit, northeastern China: insights into the structural controls on mineralization," *Journal of Earth Science*, vol. 32, no. 1, pp. 174–184, 2021.
- [16] T. Ma, G. Xiang, Y. Shi, and Y. Liu, "Horizontal in situ stresses prediction using a CNN-BiLSTM-attention hybrid neural network," *Geomechanics and Geophysics for Geo-Energy and Geo-Resources*, vol. 8, no. 5, pp. 1–26, 2022.
- [17] K. K. Zhao, P. F. Jiang, Y. J. Feng, X. D. Sun, L. X. Cheng, and J. W. Zheng, "Investigation of the characteristics of hydraulic



- fracture initiation by using maximum tangential stress criterion,” *Journal of Mining and Strata Control Engineering*, vol. 3, no. 2, article 023520, 2021.
- [18] H. Zhu, Y. Ju, C. Huang et al., “Pore structure variations across structural deformation of Silurian Longmaxi Shale: an example from the Chuandong Thrust-Fold Belt,” *Fuel*, vol. 241, pp. 914–932, 2019.
- [19] J. Xie, Q. Qin, and C. Fan, “Quantitative prediction of fracture distribution of the Longmaxi formation in the Dingshan area, China using FEM numerical simulation,” *Acta Geologica Sinica-English Edition*, vol. 93, no. 6, pp. 1662–1672, 2019.
- [20] G. Gao, S. Yang, W. Zhang, Y. Wang, W. Gang, and G. Lou, “Organic geochemistry of the lacustrine shales from the Cretaceous Taizhou Formation in the Gaoyou Sag, northern Jiangsu Basin,” *Marine and Petroleum Geology*, vol. 89, pp. 594–603, 2018.
- [21] A. Su, H. Chen, Y. X. Feng, J. X. Zhao, and A. D. Nguyen, “Multistage fracturing history in the Paleocene lacustrine shale oil reservoirs of the Subei Basin, Eastern China,” *Marine and Petroleum Geology*, vol. 144, article 105835, 2022.
- [22] J. Feng, L. Shang, X. Li, and P. Luo, “3D numerical simulation of heterogeneous in situ stress field in low-permeability reservoirs,” *Petroleum Science*, vol. 16, no. 5, pp. 939–955, 2019.
- [23] J. Liu, W. Ding, H. Yang et al., “3D geomechanical modeling and numerical simulation of in-situ stress fields in shale reservoirs: a case study of the lower Cambrian Niutitang formation in the Cen’gong block, South China,” *Tectonophysics*, vol. 712, pp. 663–683, 2017.
- [24] C. H. Fan, H. Li, Q. R. Qin, S. He, and C. Zhong, “Geological conditions and exploration potential of shale gas reservoir in Wufeng and Longmaxi Formation of southeastern Sichuan Basin, China,” *Journal of Petroleum Science and Engineering*, vol. 191, article 107138, 2020.
- [25] J. Liu, P. Chen, K. Xu, H. Yang, H. Liu, and Y. Liu, “Fracture stratigraphy and mechanical stratigraphy in sandstone: a multiscale quantitative analysis,” *Marine and Petroleum Geology*, vol. 145, article 105891, 2022.
- [26] X. Wang, H. Zhang, K. Zhang et al., “Rock breaking simulation and optimization design of multi-ridged PDC cutters,” *Journal of China University of Petroleum (Edition of Natural Science)*, vol. 46, no. 4, pp. 63–71, 2022.
- [27] Y. Chai and S. Yin, “3D displacement discontinuity analysis of in-situ stress perturbation near a weak fault,” *Advances in Geo-Energy Research*, vol. 5, no. 3, pp. 286–296, 2021.
- [28] J. Liu, W. Ding, H. Yang, P. Dai, Z. H. Wu, and G. J. Zhang, “Natural fractures and rock mechanical stratigraphy evaluation in the Huaqing area, Ordos Basin: a quantitative analysis based on numerical simulation,” *Journal of China University of Geosciences*, pp. 1–19, 2022, <http://kns.cnki.net/kcms/detail/42.1874.P.20220711.0942.004.html>.
- [29] J. Liu, L. Mei, W. Ding, K. Xu, H. Yang, and Y. Liu, “Asymmetric propagation mechanism of hydraulic fracture networks in continental reservoirs,” *GSA Bulletin*, vol. 135, no. 3-4, pp. 678–688, 2023.
- [30] K. Xu, H. Yang, H. Zhang et al., “Fracture effectiveness evaluation in ultra-deep reservoirs based on geomechanical method, Kuqa Depression, Tarim Basin, NW China,” *Journal of Petroleum Science and Engineering*, vol. 215, article 110604, 2022.
- [31] K. Xu, H. Zhang, R. Dong et al., “In situ stress distribution in cretaceous ultra-deep gas field from 1D mechanical earth model and 3D heterogeneous geomechanical model, Kuqa Depression, Tarim Basin, NW China,” *Frontiers in Earth Science*, vol. 10, article 937393, 2022.
- [32] Y. F. Yang, K. Wang, Q. F. Lv et al., “Flow simulation considering adsorption boundary layer based on digital rock and finite element method,” *Petroleum Science*, vol. 18, no. 1, pp. 183–194, 2021.
- [33] S. R. Lan, D. Z. Song, Z. L. Li, and Y. Liu, “Experimental study on acoustic emission characteristics of fault slip process based on damage factor,” *Journal of Mining and Strata Control Engineering*, vol. 3, no. 3, article 033024, 2021.
- [34] S. Yin, Q. Jia, and W. Ding, “3D paleotectonic stress field simulations and fracture prediction for marine-continental transitional facies forming a tight-sandstone reservoir in a highly deformed area,” *Journal of Geophysics and Engineering*, vol. 15, no. 4, pp. 1214–1230, 2018.
- [35] J. S. Liu, W. L. Ding, Z. K. Xiao, and J. S. Dai, “Advances in comprehensive characterization and prediction of reservoir fractures,” *Progress in Geophysics*, vol. 34, no. 6, pp. 2283–2300, 2019.
- [36] H. Li, F. Yu, M. Wang, Y. Wang, and Y. Liu, “Quantitative prediction of structural fractures in the Paleocene lower Wenchang formation reservoir of the Lufeng Depression,” *Advances in Geo-Energy Research*, vol. 6, no. 5, pp. 375–387, 2022.
- [37] H. Hu and F. Liu, “Density-functional-theory formulation of classical and quantum Hooke’s law,” *Science China Technological Sciences*, vol. 57, no. 4, pp. 692–698, 2014.
- [38] S. G. Kravchenko, O. G. Kravchenko, and C. T. Sun, “A two-parameter fracture mechanics model for fatigue crack growth in brittle materials,” *Engineering Fracture Mechanics*, vol. 119, pp. 132–147, 2014.
- [39] C. H. Fan, H. B. Xie, H. Li et al., “Complicated fault characterization and its influence on shale gas preservation in the southern margin of the Sichuan Basin, China,” *Lithosphere*, vol. 2022, no. Special 12, article 8035106, 2022.
- [40] D. A. Wood, “Predicting brittleness indices of prospective shale formations from sparse well-log suites assisted by derivative and volatility attributes,” *Advances in Geo-Energy Research*, vol. 6, no. 4, pp. 334–346, 2022.
- [41] J. Zuo, M. Yu, and S. Hu, “Experimental investigation on fracture mode of different thick rock strata,” *Journal of Mining and Strata Control Engineering*, vol. 1, no. 1, article 013007, 2019.
- [42] Z. Jia, J. Peng, Q. Lu et al., “Formation mechanism of ground fissures originated from the hanging wall of normal fault: a case in Fen-Wei Basin, China,” *Journal of Earth Science*, vol. 33, no. 2, pp. 482–492, 2022.